IRSTI 30.17.53 https://doi.org/10.26577/ijmph.2022.v13.i1.03

G.A. Ashirova[1] *, A.K. Manapova[2] , A.O. Beketaeva[1]

[1]Institute of Mathematics and Mathematical Modeling, Almaty, Kazakhstan
[2]Kazakh British Technical University, Almaty, Kazakhstan
*e-mail: gulzana.ashyrova@yandex.ru
(Received 23 February 2022; received in revised form 18 March 2022; accepted 30 March 2022)

Numerical Simulation of Particle Dynamics in the Hydrogen-Air Mixing Layer

Abstract. In this paper, supersonic plane turbulent mixing layer of gases with injection of solid particles is studied numerically. The gas phase are determined by DNS solving the multi-species Navier-Stokes equations in the Eulerian approach , and the dynamic of solid particles are traced in the Lagrangian approach. The dynamics of hydrogen – air mixing and the formation of the vortex system in the mixing layer and its effect on the distribution of solid particles in the two free-flow speeds are investigated. The study focuses on detailed analysis an influence of the vortex system in the supersonic turbulent mixing layer on the dispersion solid particles with different size. The results show that heavy particles almost do not react to vortex structures. It is revealed that medium particles tend to accumulate along the circumference of the vortex and along the braid between the two vortices. A quasi-equilibrium state with a gas flow of light particles is established.

Key words: two-phase flow, solid particles, multicomponent gas, mixing layer, Navier - Stokes equations.

Introduction

The understanding of the physics of mixing properties, ignition, and combustion, which are related to the turbulent supersonic mixing layer flow in the presence of particles, is strongly needed for the optimal design and operation of scramjet combustors.

The two-phase flows involving solid, droplet, or suspensions are investigated intensively both experimentally [1-3] and numerically [4-13]. Quite a lot of research have been devoted to the study of particle dynamics in subsonic flows [7–10]. In [7] with a two-way coupling way. It was revealed in the process of vortex rolling up and vortices pairing, the particles with different Strouhal numbers have a very different pattern of dispersion. In [9] using DNS was found that the asymmetry of the developing mixing layer leads to an increase in the number of particles moving from the upper faster flow to the lower flow. Authors [10] used two-way coupled Eulerian–Lagrangian approach have been studied the particle dynamics in a turbulent boundary layer via DNS. They found the influence of the wall on the particle velocity and distribution is significant in the near wall region but is little in the outer region.

Limited number studies of particle dispersion in a supersonic flow have been performed [11-13]. For example, authors [11] showed the particle dispersion in a spatially developing compressible mixing layer. The direct numerical simulations were performed with different Stokes numbers. It has been shown the particles tend to accumulate in the peripheries of the vortical structures with high density, low vorticity inside the mixing layer, as well as the high-density regions behind the shocklets outside the mixing layer.

The Eulerian-Lagrangian approach is used for high-speed shear layers with monodisperse, adiabatic, inertial particles in the [12] to study the interactions of particles and flow turbulence and their effect on pressure fluctuations. It was found the particle–turbulence interactions change the local pressure intensity due to the displacement of the flow (due to the particles) and significant turbulence changes.

In accordance with the above, the numerically detailed analysis and discuss the influence the vortex system in the turbulent supersonic multispecies

mixing layers on the dispersion solid particles with different size will be performed via DNS numerical simulation applying a high-order essentially nonoscillatory (ENO) scheme (Figure 1).

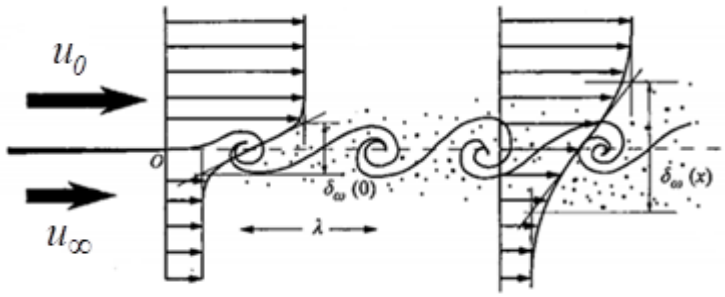

Figure 1 – Scheme of the development of the mixing layer

Model of gaseous phase

The basic equations are the system of two-dimensional Navier–Stokes equations for

a multispecies gaseous mixture, which is written in the Cartesian coordinate system in the conservative form:

$$\frac{\partial \vec{U}}{\partial t}+\frac{\partial\left(\vec{E}-\vec{E}_v\right)}{\partial x}+\frac{\partial\left(\vec{F}-\vec{F}_v\right)}{\partial z}=0, \qquad (1)$$

here the vectors $\vec{U},\vec{E},\vec{F}$ have the form

$$\vec{U}=\begin{pmatrix}\rho\\ \rho u\\ \rho w\\ E_t\\ \rho Y_k\end{pmatrix}, \quad \vec{E}=\begin{pmatrix}\rho u\\ \rho u^2+p\\ \rho uw\\ \left(E_t+p\right)u\\ \rho uY_k\end{pmatrix},$$

$$\vec{F}=\begin{pmatrix}\rho w\\ \rho uw\\ \rho w^2+p\\ \left(E_t+p\right)w\\ \rho wY_k\end{pmatrix},$$

and $\vec{E}_v,\vec{F}_v$ - the dissipative terms of the form

$$\vec{E}_v=\left(0,\tau_{xx},\tau_{xz},u\tau_{xx}+w\tau_{xz}-q_x,J_{kx}\right)^{\mathrm{T}},$$

$$\vec{F}_v=\left(0,\tau_{xz},\tau_{zz},u\tau_{xz}+w\tau_{zz}-q_z,J_{kz}\right)^{\mathrm{T}}.$$

The tensors of viscous stresses and heat fluxes are:

$$\tau_{xx}=\frac{\mu_1}{\mathrm{Re}}\left(2u_x-\frac{2}{3}\left(u_x+w_z\right)\right),$$

$$\tau_{zz}=\frac{\mu_1}{\mathrm{Re}}\left(2w_z-\frac{2}{3}\left(u_x+w_z\right)\right),$$

$$\tau_{xz}=\tau_{zx}=\frac{\mu_1}{\mathrm{Re}}\left(u_x+w_x\right),$$

$$q_z=\frac{\mu_1}{\mathrm{Pr}\,\mathrm{Re}}\cdot\frac{\partial T}{\partial z}+\frac{1}{\gamma_\infty \mathrm{M}_\infty^2}\sum_{k=1}^{N}h_kJ_{zk},$$

$$q_x=\frac{\mu_1}{\mathrm{Pr}\,\mathrm{Re}}\cdot\frac{\partial T}{\partial x}+\frac{1}{\gamma_\infty \mathrm{M}_\infty^2}\sum_{k=1}^{N}h_kJ_{xk},$$

$$J_{kx}=-\frac{\mu_1}{\mathrm{Sc}\,\mathrm{Re}}\cdot\frac{\partial Y_k}{\partial x},\quad J_{kz}=-\frac{\mu_1}{\mathrm{Sc}\,\mathrm{Re}}\cdot\frac{\partial Y_k}{\partial z},$$

where ρ is the density, u and w are the velocity components, p is the pressure, E_t is the total energy, Y_k is the mass fraction of the k^{th} species, Wk is the molecular weight of the k^{th} species ($k=1,\ldots,N$, N is the number of species in the gas mixture), Re is the Reynolds number, Pr is the Prandtl number, Sc is the Schmidt number.

The equation of state for the mixture of perfect gases may be written as

$$p=\frac{\rho T}{\gamma_\infty \mathrm{M}_\infty^2 W},$$

where $W = \left(\sum_{k=1}^{N} \frac{Y_k}{W_k} \right)^{-1}$ is the molar weight of the mixture of all gases, and $\sum_{k=1}^{N} Y_k = 1$.

The equations for the total energy have the following form:

$$E_t = \frac{\rho h}{\gamma_\infty \mathrm{M}_\infty^2} - p + \frac{1}{2}\rho\left(u^2 + w^2\right), \qquad (2)$$

where $h = \sum_{k=1}^{N} Y_k h_k$ is the mixture specific enthalpy, $h_k = h_k^0 + \int_{T_0}^{T} c_{pk} dT$ is the specific enthalpy of the k^{th} component.

The specific heats at constant pressure are computed for each component c_{pk} via the molar specific heats C_{pk} by the formula $c_{pk} = C_{pk} / W$, where C_{pk} are determined from experimental data with the aid of the fourth-order polynomial interpolation in temperature:

$$C_{pk} = \sum_{i=1}^{5} \overline{a}_{ki} T^{(i-1)},$$

where $\overline{a}_{jk} = a_{jk} T_\infty^{\,j-1}$.

The numerical values of empirical constants a_{jk} have been taken from the table JANAF [28] at normal pressure $\left(p = 1\ atm\right)$ and standard temperature $T = 293K$.

The mixture molecular viscosity is determined by Wilke's formula [14]

$$\mu_1 = \sum_{i=1}^{N} \frac{X_i \mu_i}{\Phi_i},$$

where the function Φ_i is specified in the form

$$\Phi_i = \sum_{r=1}^{N} X_r \left[1 + \sqrt{\frac{\mu_i}{\mu_r}} \left(\frac{W_r}{W_i} \right)^{1/4} \right]^2 \left[\sqrt{8} \sqrt{1 + \frac{W_i}{W_r}} \right]^{-1},$$

μ_i is the molecular viscosity of the i^{th} component, it is calculated by the formula

$$\mu_i = \frac{\mu_{i\infty}}{\mu_{\Lambda\infty}} \sqrt{W_i T_\infty},$$

where $\mu_{i\infty} = 2.6693 \cdot 10^{-7} \frac{\sqrt{W_{i\infty} T_\infty}}{\sigma_i^2 \Omega_i^{(2.2)^*}\left(T_i^*\right)}$, $\mu_{l\infty} = \sum_{i=1}^{N} \frac{X_i \mu_{i\infty}}{\Phi_i}$, σ_i is the collision diameter of the i^{th} component, the values of components are presented in the work [14]: σ_1 = 2.63, σ_2 = = 3.30, σ_3 = 3.5, σ_4 = 3.050, σ_5 = 0.50, σ_6 = 0.560, σ_7 = 3.50, $\Omega_i^{(2.2)^*}$ is the integral of collisions for the momentum transfer, $T_i^* = kT/\varepsilon_i$ is the reference temperature, ε_i / k is the parameter of the potential function of the intermolecular interaction. According to the work [15], $\Omega_i^{(2.2)^*}\left(T_i^*\right) = 1$.

The turbulent flow is assumed quasi-two-dimensional, and the system of the Navier–Stokes equations is solved with the aid of the two-dimensional DNS approach without using the additional closing turbulence models.

Disperse phase model

The following assumptions are adopted for the dynamic particles: the particles are the spheres of the same size; the interaction of particles with one another is not taken into account; the particles motion does not affect the gas flow; the forces of Saffman and Magnus do not consider hence the small aluminum particles are considered. In accordance with these assumptions, the equations for the motion trajectory $\left(\vec{x}_\mathrm{p}\right)$ and the velocity $\left(\vec{u}_\mathrm{p}\right)$ of particles are written as follows:

$$\frac{d}{dt}\vec{x}_p = \vec{u}_p, \qquad (3)$$

$$m\frac{d}{dt}\vec{u}_p = \vec{F}_p + mg,$$

where $m = \frac{4}{3}\pi r_\mathrm{p}^3 \rho_\mathrm{p}$ is the mass of a spherical

solid particle, ρ_p is the density of the solid particle of the p^{th} component, F_p is the drag force acting from the gas side on the particle of radius r_p which is determined as

$$\vec{F}_p = C_{\mathrm{D}} \frac{1}{2} \pi r_p^2 \rho \left|\vec{u} - \vec{u}_p\right| \left(\vec{u} - \vec{u}_p\right),$$

here C_{D} is the drag coefficient, μ is the coefficient of the gas dynamic viscosity.

For the case of a turbulent flow around a particle at $Re > 1$, different formulas are used for the drag coefficient C_{D} (based on the Stokes formula $C_{\mathrm{D}} = 24/\mathrm{Re}$) with regard for gas properties and motion regime. The most known formula is the one proposed in the [16], which is also used in the present work in the form:

$$C_{\mathrm{D}} = \begin{cases} \dfrac{24}{\mathrm{Re_p}}\left(1 + \dfrac{1}{6}\mathrm{Re_p^{2/3}}\right), & \mathrm{Re_p} \le 1000, \\ 0.424, & \mathrm{Re_p} > 1000, \end{cases}$$

where $\mathrm{Re}_p = \dfrac{2\rho\left|\vec{u} - \vec{u}_{\mathrm{p}}\right|}{\mu}$ is the Reynolds number built in terms of the particle radius r_p.

The governing equations (1)–(3) are written in dimensionless form. As the non-dimensionalization parameters, the following reference values of the upper flow have been taken: $u_\infty, \rho_\infty, T_\infty, Y_{k\infty}$; the pressure and total energy are related to the value $\rho_\infty u_\infty^2$, the reference length is the vorticity inlet thickness $\delta_\omega = \dfrac{(u_\infty - u_0)}{(\partial u/\partial z)_{\max}}$. The time scale is defined as $t \approx \delta_\omega / u_\infty$. The same parameters as for the gaseous phase are taken for disperse phase at the non-dimensionalization.

Initial and boundary conditions

The parameters of gas flows are specified at the inlet as follows:

the upper flow

$$u = u_0 = \mathrm{M}_0\sqrt{\gamma_0 R T_0 / W_0},\ w = 0,\ p = p_0,\ T = T_0,$$
$$Y_k = Y_{k0} \text{ at } x = 0,\ 0 \le z < H_1,$$

the lower flow

$$u = u_\infty = \mathrm{M}_\infty\sqrt{\gamma_\infty R T_\infty / W_\infty},\ w = 0,\ p = p_\infty,$$
$$T = T_\infty,\ Y_k = Y_{k\infty}$$
$$\text{at } x = 0,\ H_1 + \delta \le z < H_2,\ H_z = H_1 + \delta + H_2.$$

H_z is the height and H_x – the length of the region under consideration.

At the inlet, the particle velocities are set equal to the flow velocities at the injection point. In a thin mixing layer, the initial velocity u are determined by the hyperbolic tangent function

$$\varphi(\mathrm{z}) = 0.5\left(\varphi_0 + \varphi_\infty\right) + \\ +0.5\left(\varphi_0 - \varphi_\infty\right)\tanh\left(0.5z/\delta_\theta\right), \tag{4}$$

where

$$\varphi = (u, Y_k, T),$$
$$\delta_\theta(x) = \int_{H_1/2}^{H_2/2} \left(\rho\left(\tilde{u} - u_\infty\right)\left(u_0 - \tilde{u}\right) \Big/ \left(\rho_\infty \Delta u^2\right) dz\right)$$

$\delta_\theta(x)$ is the thickness of the momentum loss, $\tilde{u} = \left(u - u_\infty\right)/\Delta u$ is the gas mean velocity, $\Delta u = (u_\infty - u_0)$ is the difference of inlet velocities. The initial conditions are set in the same way as the inlet boundary conditions. The non-reflecting boundary conditions are specified at the outlet, bottom, and top boundaries, where the gas fluxes and perturbations pass through the boundary and do not reflect back [17]. The inflow perturbation at the inlet the boundary conditions, in which one adds for the velocity fields $\vec{u}(z)$ a random phase u_{dist} :

$$\vec{u} = \vec{u}(z) + \vec{u}_{distr},$$

where

$$\vec{u}_{distr} = \sum_{m=1}^{3} A_m \cdot \Delta u \cdot Gaussian(z) \cdot \sin(\omega_m \cdot t + \alpha), \tag{5}$$

here $\vec{u}(z)$ is the hyperbolic tangent function defined by formula (4). The A_m is the perturbation amplitude, which is satisfying the condition that the given product $A_m \Delta u$ must be equal to 0.1–0.2% of the maximum velocity of gases at the inlet. The perturbation frequency ω_m are taken: $\frac{2\pi}{18} \le \omega_m \le \frac{2\pi}{10}$ The $Gaussian(z)$ is the Gauss function the maximum value of which is equal to unity at z = 0and α is a random number.

Method of solution

Numerical solution of the system of equations (1), i.e., the gaseous phase, is carried out in two stages. At the first stage, one computes the vector of the thermodynamic parameters $\vec{U}$ and at the second stage, the mass fraction of the k^{th} species $Y_k = 1,7.$ For a more detailed consideration of the flow at the inlet of the mixing layer, the grid clustering is introduced with the aid of the following transformations:

$$\xi = \xi(x),\ \eta = \eta(z). \tag{6}$$

In this case, the system of equations (1) in generalized coordinates is written as:

$$\frac{\partial \tilde{U}}{\partial t} + \frac{\partial \tilde{E}}{\partial \xi} + \frac{\partial \tilde{F}}{\partial \eta} = \frac{\partial \tilde{E}_{v2}}{\partial \xi} + \frac{\partial \tilde{E}_{vm}}{\partial \xi} + \frac{\partial \tilde{F}_{v2}}{\partial \eta} + \frac{\partial \tilde{F}_{vm}}{\partial \eta} \tag{7}$$

where

$$\tilde{U} = \frac{1}{J}\vec{U},\ \tilde{E} = \left(\frac{\xi_x}{J}\right)\vec{E},\ \tilde{F} = \left(\frac{\eta_z}{J}\right)\vec{F},$$

$$\tilde{E}_{v2} = \left(\frac{\xi_x}{J}\right)\vec{E}_{v2},\ \tilde{E}_{vm} = \left(\frac{\xi_x}{J}\right)\vec{E}_{vm},$$

$$\tilde{F}_{v2} = \left(\frac{\eta_z}{J}\right)\vec{F}_{v2},\ \tilde{F}_{vm} = \left(\frac{\eta_z}{J}\right)F_{vm},$$

$J = \frac{\partial(\xi,\eta,\zeta)}{\partial(x,z,y)}$ – Jacobian transformation.

The numerical solution algorithm is based on a finite-difference third-order ENO scheme, which have been described in detail in the work [18-21].

Using the known values of the original variables and equation (2), the temperature field is computed with the aid of the equation

$$f(T) = E_t - \frac{\rho}{\gamma_\infty \mathrm{M}_\infty^2 W}\left(H(T) - R\,T\right) - \frac{1}{2}\rho\left(u^2 + w^2\right) = 0, \tag{8}$$

where H is the molar enthalpy of the gas mixture. The solution of the algebraic equation (8) for temperature is found by the Newton–Raphson iteration method [15].

The system of the ordinary differential equations (3) for the particles is solved with the explicit second order Euler method.

Results and Discussion

For the verification of the numerical method, the test problem of the shear flow of the multispecies gases without particles is solved. The numerical results are compared with computations of the [22]. For that the test problem is performed with follows conditions: the inflow lower air are a mixture of nitrogen (N_2) and oxygen (O_2) $Y_{O_2} = 0.232,$ $Y_{N_2} = 0.768$; the inflow upper flow the mixture of nitrogen (N_2) and hydrogen (H_2) $Y_{H_2} = 0.1,$ $Y_{N_2} = 0.9$ .The flow parameters for air – M_∞ = 2.1, T_∞ = 2000K, p_∞ = 101321Pa, for nitrogen-hydrogen mixture – M_∞ = 2, T_∞ = 2000K, p_∞ = 101321Pa. The convective Mach number $M_c = (u_c - u_\infty)/a_\infty,$ $u_c = (a_\infty u_0 + a_0 u_\infty)/(a_\infty + a_0)$, amounted here to M_c = 0.38. The dimensionless length and height of the domain are H_x = 350, H_z = 120. The geometric parameters of the problem under consideration are dimensioned to the initial thickness of the momentum loss which at the entrance is 9.35x10$^5 m$. For numerical simulation, the finest grid spacing is specified as non-dimensional 0.03 around the mixing layer center and the cell numbers in the x and z directions are 626x241.

Figure 2 shows turbulent shear stresses $\sigma_{uu} = \sqrt{\overline{u''^2}}/\Delta u$ и $\sigma_{uw} = \sqrt{\overline{u''w''}}/\Delta u$ in the sections x = 320. Turbulent characteristics, such as the intensity of turbulence and Reynolds stresses have quantitatively small discrepancies.

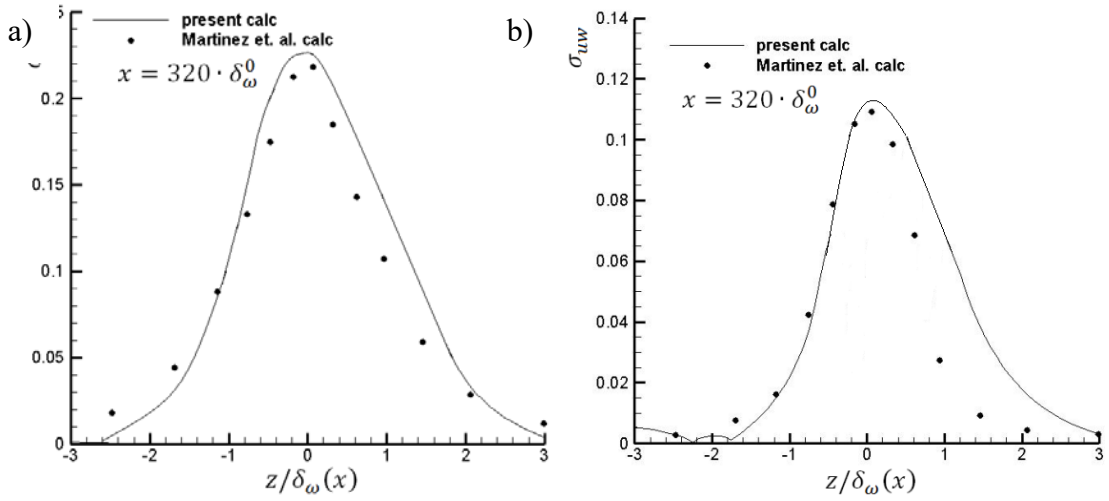

Figure 2 - Comparison of the calculated data obtained by the ENO scheme (solid line) and the numerical results of Martinez et al. [22] (circle points) for the profiles of turbulent shear stresses at section $x = 320\delta_\omega^0$, a) σ_{uu} , b) σ_{uw}

The numerical simulation of the posed problem was carried out for the dimensionless domain $H_x = 320, H_z = 80.$ The inflow lower air with $Y_{O_2} = 0.232, Y_{N_2} = 0.768$ and upper flow (the mixture of nitrogen (N_2) and hydrogen (H_2)) with $Y_{H_2} = 1,\ Y_{N_2} = 0$ are taken. The Mach number of injected upper hydrogen-nitrogen mixture is $M_0 = 2$ and for lower air $M_\infty = 1.5$. The gas flow temperature is adopted equal $T_0 = 600,\ T_\infty = 1200$, the pressure $p_0 = p_\infty = 1\ atm$. The aluminum particles of the three sizes of diameters $d = 95\mu m,\ d = 9{,}5\mu m,\ d = 1{,}9\mu m$ are injected from five holes at the entrance simultaneously which is located near the center of the mixture layer $(x = 0, z = 20, 30, 40, 50, 60).$

The graphs below show non-stationary vortex system obtained by numerical simulation. The dynamics of hydrogen – air mixing are illustrated in Figure 3 by instantaneous hydrogen concentration and streamlines at different time: $a)\ t = 100,\ b)\ t = 200,\ c)\ t = 400,\ d)\ t = 600,$ $e)\ t = 1000.$

As follows from figures, a significant curvature of the streamlines begins at time $t = 100$, in the cross section $x = 50$ as a result of flow instability (Figure 3a). It is confirmed by the distribution of hydrogen contours, where formation of vortices begins in this section (Figure 3a) and the whirling vortex captures the airflow and simultaneously the hydrogen mixture takes out leading to the mixing layer expands. Over time, the number of arising vortices increases conducting to a considerable growth of the mixing layer in the hydrogen-air mixture. Therefore, the intensification of vortex twisting closed hydrogen zones are formed in the centers of their rotation (Figure 3d)

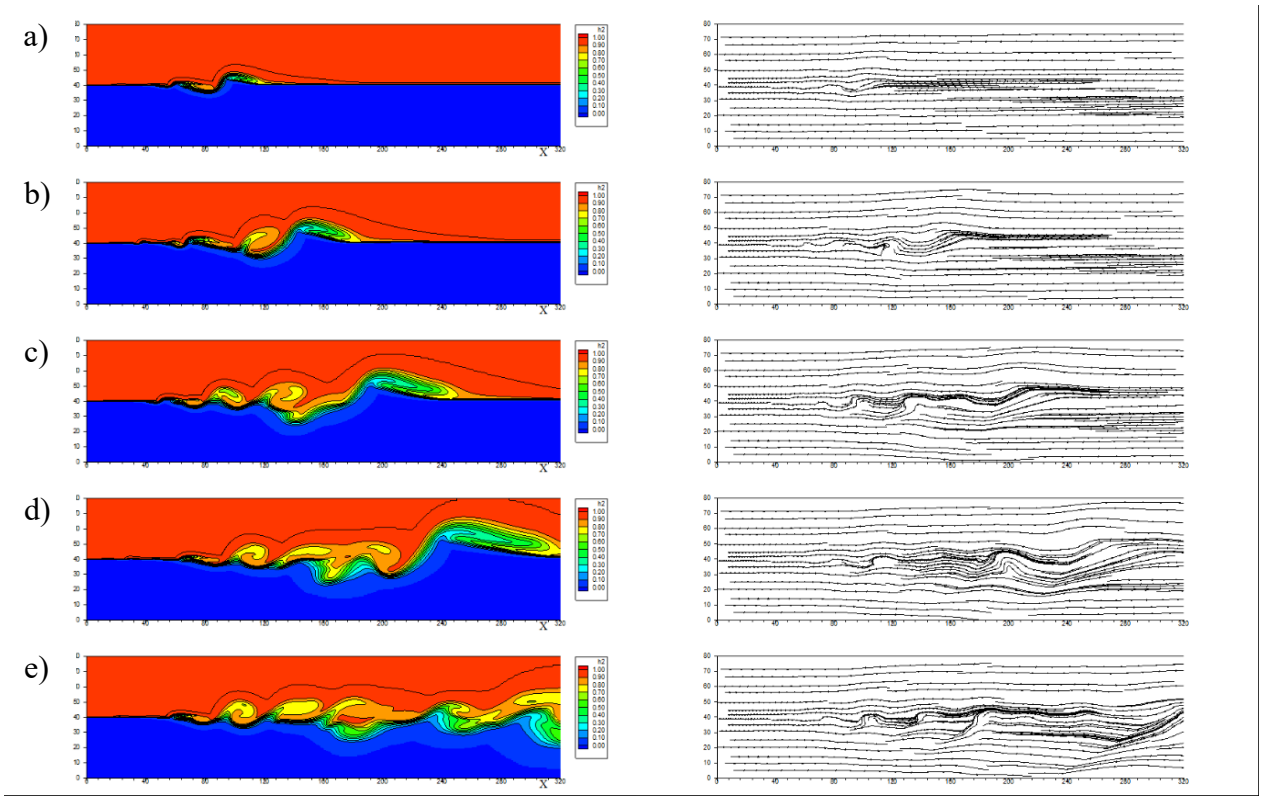

Figure 3–Distribution of the hydrogen mass concentration (left) and distribution of streamlines (right) at different time: *a*) $t=100$, *b*) $t=200$, *c*) $t=400$, *d*) $t=600$, e) $t=1000$

The dynamics of vortex bubbles and entrained particles (particle dispersion over time) is shown in Figure 4, which illustrates instantaneous vorticity contours and particle trajectories at various moments

$$a)\ t=100,\ b)\ t=200,\ c)\ t=400,$$

$$d)\ t=600,\ e)\ t=1000.$$

Numerical experiments reveal that neighboring vortices merge (pair) and form larger ones at moments of time $t=200, t=400, t=600$ (Figure 3 b – d). Apparently, each such merging lead to the entrainment of the non-whirling gas in the mixing layer thereby to the thickening of mixing layer. The generation of three vortex systems is observed at a distance from $x=40$ to $x=180$ by the moment of time $t=200$ in Figure 4b and the number of vortices grow to 4 and 5 at times $t=400$ and $t=600$, respectively. A stable turbulent vortex structure forming with time $(t=1000)$ and consisting of seven vortices is shown in Figure 4 e.

The particle distribution provided in the same figure demonstrate that particles injected into the rapid upper flow move much faster compared to particles injected into the slower lower flow at the initial time $t=100$. Hence, for example, the particles that started moving from the inlet point $x=0$ and injected at the height $z=50,60$ propagate by the moment of time until the cross section $x=200$ .Part of them gets into the vortex zone $(x=80\div160)$ and the trajectories of these particles become circular.

However, the slow moving particles (the particles injected from lower stream at height $(z=20, z=30)$ are still not captured by vortices and continue moving along their own trajectories and reach the position $x=80$ by the moment of time $t=100$. It follows from Figure 4 b – d, e that the particles are entrained completely into the vortex zone of the mixing layer over time, despite that dispersion of particles injected into the slower flow is much less compared to the particles which move in the faster flow.

As you can see from numerical experiments, that particles have tendency to accumulate in the periphery of vortex structures, which is visible from Figure 4, therefore, they are captured by vortices practically uniformly.

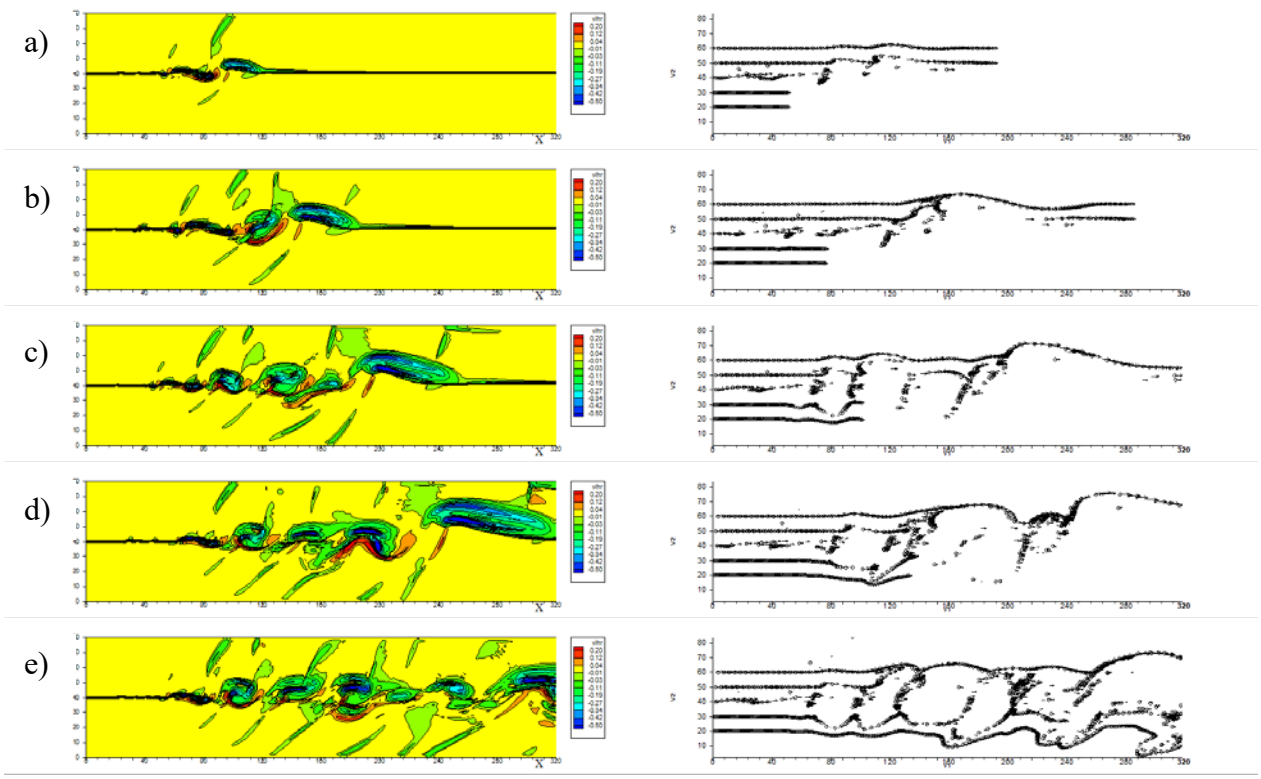

Figure 4–Distribution of vorticity contours (left) and distribution of particles (right) at different time *a*) $t = 100$, *b*) $t = 200$, *c*) $t = 400$, *d*) $t = 600$, e) $t = 1000$

The above result shows that particles injected into the faster flow are more dispersed than particles injected into the slow flow, which are in qualitative agreement with the observed behavior of particles in the developing mixing layer. Despite that, the mixing of particles between the two flows is shifted towards low velocity. It is confirmed in Figure 5, where presented the quantitative distribution of particles in the upper (Figure 5a) and in the low (Figure 5 b) mixing layers along the centerline of the x – axis at time $t = 1000$.

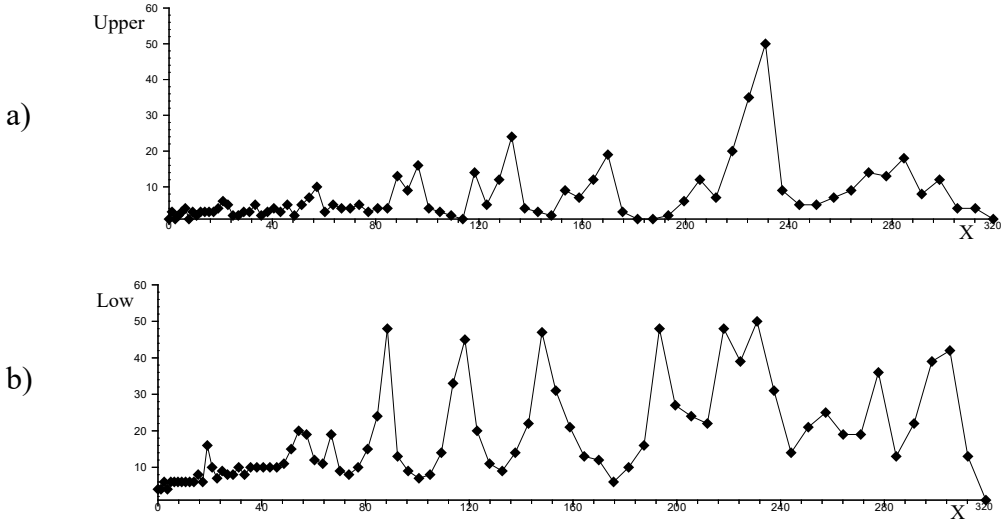

Figure 5 – Quantitative distribution of particles of the upper (a) and lower (b) flows over the cross section x at time $t = 1000$.

The number of particles is determined as follows:

$$N_{\text{rms}}(x) = \left(\sum_{i=1}^{N_{\text{cp}}} \frac{N_i(x)^2}{N_{\text{cp}}} \right)^{1/2},$$

here N_{cp} is the total number of grid cells, $N_i(x)$ is the number of particles in the i^{th} cell. As is seen in the Figure 5, the number of particles in the lower airflow is larger in comparison with their number in the upper flow of the hydrogen-nitrogen mixture.

Figures 6-7 provide numerical results with three different particle sizes of $a) d = 95\ mkm$ (heavy), $b) d = 9.5\ mkm$ (medium), $c) d = 1.85\ mkm$ (light). The following shows an analysis of the influence of particle sizes on the dispersion of particles and their location in the turbulent mixing layer.

Figure 6 shows the motion pattern of particles with different diameters $a)\ d = 95,\ b)\ d = 9.5,\ c)\ d = 1.85$ at the time points $t = 100$ (left) and $t = 200$ (right). Fluid flow practically does not affect the distribution of heavy particles due to the absence of large stable structures at the time $t = 100$ (Figure 6a).

However, medium and light particles are already transported through the first vortices, which leads to a curvature of the particle's trajectories, which can be observed in Figure 6 b, c. It can be seen here that the particles are moving away from the vortex cores, accumulating in the areas surrounding the vortices and in the areas of the braid. The trajectories of heavy particles do not change at time $t = 200$ (Figure 6), even though larger vortices are created at this time (see Figure 3), this is since the intrinsic momentum of the particles is significantly greater than the momentum generated by the vortices. In this case, medium and light particles are attracted by large vortices from large distances to the mixing layer. The particle distribution becomes non-uniform and a large area of the vortex core still has not particles.

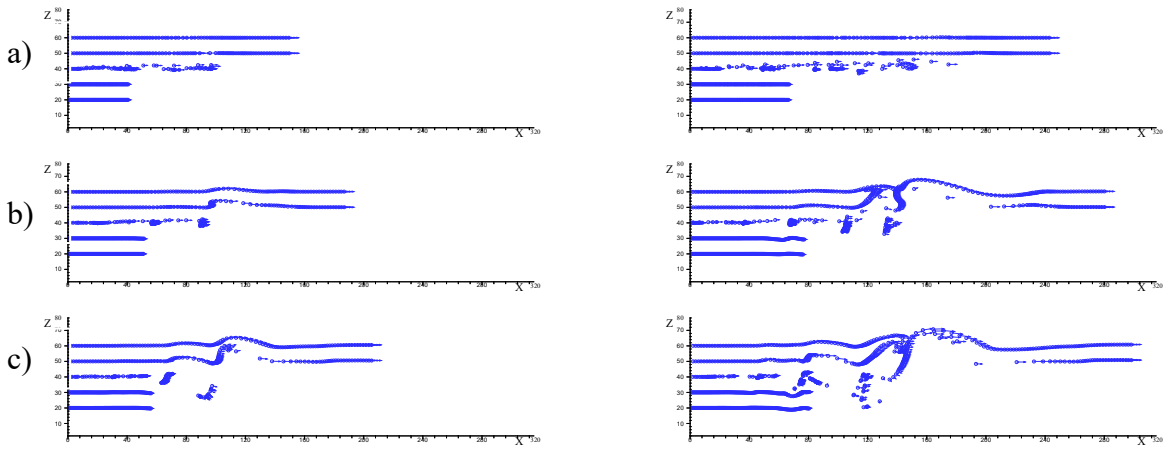

Figure 6 – Particle's trajectories at times $t = 100$ (left) and $t = 200$ (right) $a)\ d = 95,\ b)\ d = 9.5,\ c)\ d = 1.85$

Figure 7 demonstrated dispersion of particles with different diameters $a)\ d = 95,\ b)\ d = 9.5,\ c)\ d = 1.85$ at times $t = 600$ and $t = 1000$. One can see that the movement and distribution of particles in the mixing layer are strongly influenced by size. Heavy particles move along rectilinear trajectories. The particles almost do not react to the turning and rotation of large vortex structures, a small dispersion is observed only downstream.

However, medium-sized particles tend to accumulate along the circumference of the vortex and along the braid between the two vortices, which leads to appearing some "empty" areas where the solid particles are almost not observed (Figure 7b). This is due to the effects of deformation of the flow field in combination with centrifugal effects. This result means that the simulated flow can create almost linearly ordered particle dispersion structures at certain particle sizes.

On the contrary, light particles are carried throughout the flow field, including the vortex nuclei, which is clearly seen in the cross section $160 < x < 320$ (Figure 7c). Since these particles react faster to flow changes, the structure of the particle dispersion resembles the flow vortex structure. In other words, light particles are in a quasi-equilibrium state with the gas.

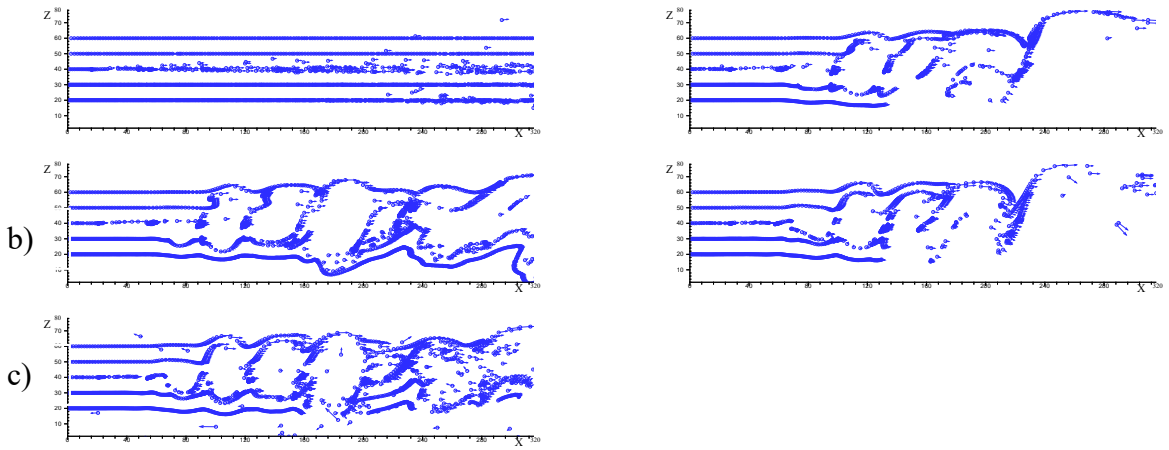

Figure 7 - Particles trajectories at times $t = 600, t = 1000$
a) $d = 95$, *b*) $d = 9.5$, *c*) $d = 1.85$

Conclusion

A supersonic plane turbulent mixing layer of gas–particles for the flow of two parallel streams of hydrogen (upper high–speed) and air (lower low–speed) is numerically studied. It was found that the hydrogen – air mixing are generated non-stationary vortex system. It is revealed that neighboring vortices pair and form larger ones over time. Thereby, mixing layer is thickened. The particle distribution indicates that the particles injected into the fast upper stream move much faster than the particles injected into the slower lower stream. Particles are eventually completely entrained into the vortex zone of the mixing layer, even though the dispersion of particles injected into a slower flow is much smaller than particles that move in a faster flow. Numerical experiments show that particles tend to accumulate on the periphery of vortex structures. Numerical results with three different particle sizes at various time are also examined. It is confirmed that the movement of particles and their distribution in the mixing layer are strongly influenced by size. Heavy particles almost do not react to vortex structures. At the same time, medium particles tend to accumulate along the circumference of the vortex and along the braid between the two vortices. On the contrary, particles with a small diameter are carried by the gas flow throughout the flow field, including the vortex cores.

References

1. Kulick J.D., Fessler J.R., Eaton J.K. “Particle response and turbulence modification in fully developed channel flow”. *J. Fluid Mech*. 277, 109–34. (1994)

2. Simakov N.N., “Experimental verification of the early crisis of drag using a single sphere”. *Tech. Phys*. 55, 7. (2010): 913–919.

3. Muste M., Parthasarathy R.N., Patel V.C. “Discriminator laser Doppler velocimetry for measurement of liquid and particle velocities in sediment-laden flows”. *Exp. Fluids*. 22. (1996): 45–56.

4. Lazaro B.J., Lasheras J.C. “Particle dispersion in the developing free shear layer”. *Part 1, Journal Fluid Mechanics*. 143. (1992): 235-247.

5. Lazaro B.J., Lasheras J.C. “Particle dispersion in the developing free layer”. *Part 2, Journal Fluid Mechanics*. 235. (1992): 179-185.

6. Pakhomov M.A., Terekhov V.I. “Solid particle spreading in gas-dispersed confined swirling flow. Eulerian and Lagrangian approaches”. *Thermophysics and Aeromechanics*. 24, 3. (2017): 325–338.

7. Lin J.Z., Lin J., Shao X.M., et al. “Research on particle dispersion in a plane-mixing layer with

coherent structure". *Acta Mech Sinica*. 19. (2003): 535–542.

8. Aggarwal S.K., Yapo J.B., Grinstein F.F., Kailasanath K. "Numerical simulation of particle transport in planar shear layers". *Comp. Fluids*. 25, 1. (1996): 39–59.

9. Hu Z., Luo X., Luo K.H. "Numerical simulation of particle dispersion in a spatially developing mixing layer". *Theoret. Comput. Fluid Dyn.*. 15, 6. (2002): 403–420.

10. Luo K., Dai Q., Liu X., Fan J. "Effects of wall roughness on particle dynamics in a spatially developing turbulent boundary layer". *Int. J. Multiphase Flow*. 111. (2018):414-421.

11. Dai Q., Jin T., Luo K., Fan J. "Direct numerical simulation of particle dispersion in a three-dimensional spatially developing compressible mixing layer". *Phys. Fluids*. 30. (2018): 56-78.

12. Buchta D.A., Shallcross G., Capecelatro J. "Sound and turbulence modulation by particles in high-speed shear flows". *J. Fluid Mech*. 875. (2019): 254-285.

13. Ren Zh., Wang B., Zheng L. "Numerical analysis on interactions of vortex, shock wave, and exothermal reaction in a supersonic planar shear layer laden with droplets". *Physics of Fluids*. 30. (2018).

14. Lapin Yu.V., Strelets M.Kh. "Internal Flows of Gas Mixtures". *Nauka*. (1989).

15. Kee R., Rupley F.M., Miller J.A. "CHEMKIN-II: a Fortran chemical kinetic package for the analysis of gas-phase chemical kinetics". *Sandia Report SAND89-8009B*. (1989).

16. Chein R., Chung J.N. "Effects of vortex pairing on particle dispersion in turbulent shear flows". *Multiphase Flow*. 13. (1987): 775-785.

17. Poinsot T.J., Lele S.K. "Boundary conditions for direct simulation of compressible viscous flows". *J. Comp. Phys*. 101, 1. (1992): 104-129.

18. Beketaeva A.O., Naimanova A.Zh. "Numerical study of spatial supersonic flow of a perfect gas with transverse injection of jets".

19. *Journal of Applied Mechanics and Technical Physics*. 52. (2011): 896-904.

20. Beketaeva A.O., Bruel P., Naimanova A. Zh. "Vortical structures behind a transverse jet in a supersonic flow at high jet to crossflow pressure ratios". *Journal of Applied Mechanics and Technical Physics*. 56, 5. (2015): 777-788.

21. Beketaeva A.O., Moisseyeva Ye.S., Naimanova A. Zh. "Numerical simulations of shock-wave interaction with a boundary layer in the plane supersonic flows with jet injection". *Thermophysics and Aeromechanics*. 23, 2. (2016):173-183.

22. Beketaeva A.O, Bruel P., Naimanova A.Zh. "Detailed Comparative Analysis of Interaction of a Supersonic Flow with a Transverse Gas Jet at High Pressure Ratios." *Technical Physics*. 64, 10. (2009): 1430–1440.

23. Martinez Ferrer P.J., Lehnasch G., Mura A. "Direct numerical simulations of high speed reactive mixing layers". *J. Physics: Conf. Ser*. 395. (2012).